Structural Engineering and Mechanics, *Vol. 60, No. 5 (2016) 781-794*
DOI: http://dx.doi.org/10.12989/sem.2016.60.5.781

Experimental investigation of multi-layered laminated glass beams under in-plane bending

Xiaokun Huang[1], Qiang Liu*[1], Gang Liu[1], Zhen Zhou[2] and Gang Li[3]

[1]*China Academy of Building Research, Beijing, China*
[2]*Kuraray (Shanghai) Co. Inc., China*
[3]*Fuxin Special Glass Co. Inc., China*

(Received February 5, 2016, Revised July 15, 2016, Accepted September 21, 2016)

Abstract. Due to its relatively good safety performance and aesthetic benefits, laminated glass (LG) is increasingly being used as load-carrying members in modern buildings. This paper presents an experimental study into one applicational scenario of structural LG subjected to in-plane bending. The aim of the study is to reveal the in-plane behaviors of the LG beams made up of multi-layered glass sheets. The LG specimens respectively consisted of two, three and four plies of glass, bonded together by two prominent adhesives. A total of 26 tests were carried out. From these tests, the structural behaviors in terms of flexural stiffness, load resistance and post-breakage strength were studied in detail, whilst considering the influence of interlayer type, cross-sectional interlayer percentage and presence of shear forces. Based on the test results, analytical suggestions were made, failure modes were identified, corresponding failure mechanisms were discussed, and a rational engineering model was proposed to predict the post-breakage strength of the LG beams. The results obtained are expected to provide useful information for academic and engineering professionals in the analysis and design of LG beams bending in-plane.

Keywords: laminated glass beam; in-plane bending; shear; multi-layered; post-breakage strength

1. Introduction

Laminated glass (LG) consists of two or more glass sheets bonded together by elastomeric interlayer materials, and is widely applied in modern buildings thanks to its good safety and security performance. Unlike monolithic glass, the fragments of LG can be retained to the interlayer in case of breakage and thus the risk of injuries is reduced. Due to this benefit, in recent years, the role of architectural LG has been gradually extended from traditional secondary elements (e.g. windows and curtain walls) to load-carrying members (Ledbetter, Walker *et al*. 2006).

Structural LG can be used as plates or beams, respectively carrying loads normal or in parallel to their plane. In the literature, extensive studies have been reported for the structural behaviors of LG subjected to out-of-plane bending (Behr, Minor *et al*. 1993, Duser, Jagota *et al*. 1999, Seshadri, Bennison *et al*. 2002, Kott and Vogel 2003, Aşik and Tezcan 2005, Foraboschi 2007, Callewaert,

*Corresponding author, Ph.D., E-mail: QXL393@gmail.com

Copyright © 2016 Techno-Press, Ltd.
http://www.techno-press.org/?journal=sem&subpage=8 ISSN: 1225-4568 (Print), 1598-6217 (Online)

Belis *et al*. 2012, Huang, Liu *et al*. 2014a, b, Huang, Liu *et al*. 2015). From these studies, it is known that the mechanical properties of interlayer materials play a decisive role in the structural performance of LG plates. In contrast, research on LG subject to in-plane bending is relatively limited to date. According to different failure mechanisms, the existing research for LG beams bent in-plane may be generally categorized into two groups, i.e., one is focused on their out-of-plane behaviors (such as buckling), and the other is committed to their in-plane behaviors (such as cross-sectional resistance and post-breakage performance). Evidently, the out-of-plane behaviors govern the design of LG beams with high slenderness ratios, whereas the in-plane behaviors are more crucial for the design of the LG beams with sufficient lateral restraints. Luible and Crisinel (2006), Amadio and Bedon (2010), Belis, Bedon *et al*. (2013) have experimentally and analytically investigated the buckling problems of the slender LG beams. Belis, Depauw *et al*. (2009) reported an experimental investigation on the behaviors of the laterally restrained LG beams made up of two glass sheets bonded with SentryGlas® Plus (SGP) interlayer (DuPont 2008), and found that the SGP LG beams had limited post-failure performance. Biolzi, Cattaneo *et al*. (2010) experimentally studied the progressive failure mechanisms of the laterally restrained polyvinyl butyral (PVB) and SGP LG beams made up of one internal annealed glass sheet and two external tempered glass sheets. They found that as loads increased the first crack took place on the annealed glass while the beams still had appreciable post-breakage capacities, especially for the beams with SGP interlayer.

In engineering practice, thick and deep LG beams are often required in circumstances where relatively heavy loads are imposed on. Since an individual glass sheet is usually manufactured in standard thicknesses of between 2 to19 mm (Wurm 2007), a heavy duty LG beam normally consists of multi-layered glass sheets, e.g. three glass sheets or more. Due to the brittle nature of glass, heavy duty LG beams must have sufficient stiffness and load resistance under normal unbroken conditions, as well as adequate post-breakage strength in case of accidental scenarios (Bos and Veer 2007). In comparison with the LG made up of two plies of glass, heavy duty LG beams often have higher cross-sectional interlayer percentages. Considering that the tensile strengths of typically used interlayer materials (such as PVB interlayer and SGP interlayer) have the same order of magnitude as the tensile strength of glass (Belis, Depauw *et al*. 2009), it is worthwhile assessing whether and how the interlayers will affect the structural behaviors of heavy duty LG beams in terms of flexural stiffness, load resistance and post-breakage strength. In addition to this, heavy duty LG can be applied as cantilever or continuous beams. In such loading scenarios, high bending and shear act simultaneously at support points. Due to a lack of detailed study, it is not yet known whether the combination of shear stress and bending stress can lead to any significant further reduction in the load resistance of the LG beams.

Reported in this paper are a series of experiments conducted with the objective of answering the above questions. The investigated LG beams were respectively made up of two, three and four annealed glass sheets. The interlayer materials used were SGP and PVB. The cross-sectional interlayer percentages were in a range from 6%~18%. The LG beam specimens were laterally restrained and subjected to short term three-point bending at room temperature. The ratio of shear span to depth of beam ranged from 2.5~5.0. The conclusions obtained are expected to provide useful and practical information for both academic and practitioners in the analysis and design of laterally restrained heavy duty LG beams sustaining in-plane short-term duration loads at room temperature.

Table 1 Overview of test specimens

Specimens	Interlayer material	Interlayer thickness (mm)	Effective Span (mm)	Depth (mm)	Glass thickness (mm)	Shear span ratio	Number of specimens
MV-1SG-150	SGP	1.78	1500	150	12+12	5.00	2
MV-2SG-150	SGP	1.78×2	1500	150	8+8+8	5.00	2
MV-3SG-150	SGP	1.78×3	1500	150	6+6+6+6	5.00	2
MV-1SG-200	SGP	1.78	1500	200	12+12	3.75	2
MV-2SG-200	SGP	1.78×2	1500	200	8+8+8	3.75	2
MV-3SG-200	SGP	1.78×3	1500	200	6+6+6+6	3.75	2
MV-1SG-300	SGP	1.78	1500	300	12+12	2.50	2
MV-2SG-300	SGP	1.78×2	1500	300	8+8+8	2.50	2
MV-3SG-300	SGP	1.78×3	1500	300	6+6+6+6	2.50	2
MV-1PVB-150	PVB	1.52	1500	150	12+12	5.00	2
MV-3PVB-150	PVB	1.52×3	1500	150	6+6+6+6	5.00	2
MV-1PVB-300	PVB	1.52	1500	300	12+12	2.50	2
MV-3PVB-300	PVB	1.52×3	1500	300	6+6+6+6	2.50	2

2. Test program

The experimental program comprised a total of 26 tests conducted in the State Key Laboratory of Building Safety and Environment at the China Academy of Building Research.

2.1 Specimens

An overview of the test specimens is presented in Table 1. The test specimens were labeled in an order indicating the loading condition (combined bending and shear stresses), number and type of interlayer, and section depth of the glass plies. Two duplicated tests were carried out for each type of the LG specimen. The LG specimens consisted of annealed float glass sheets laminated together by SGP or PVB interlayer. The SGP LG specimens were of three different depths, i.e. 150, 200 and 300 mm. The PVB LG specimens were of two different depths, i.e. 150 and 300 mm. All the LG specimens were of a constant effective span length of 1500 mm. The ratio of shear span to depth (defined as 'shear span ratio' hereafter) of the specimens ranged from 2.5 to 5.0. The shear span referred to the distance from the loading point to one of the support points. All of the LG specimens had a constant nominal overall glass thickness of 24 mm. The SGP LG specimens were respectively made up of two, three and four plies of glass, with the corresponding individual glass thickness of 12, 8 and 6 mm. The PVB LG specimens were respectively made up of two and four plies of glass, with a corresponding individual glass thickness of 12 and 6 mm. The individual nominal thickness of the SGP and PVB interlayer was 1.78 and 1.52 mm, respectively. The nominal cross-sectional areas of the interlayer accounted for approximately 6%~18% of the overall cross-sectional areas of the beams. The edges of the LG specimens were all fine polished to minimize flaws.

2.2 Test set-up

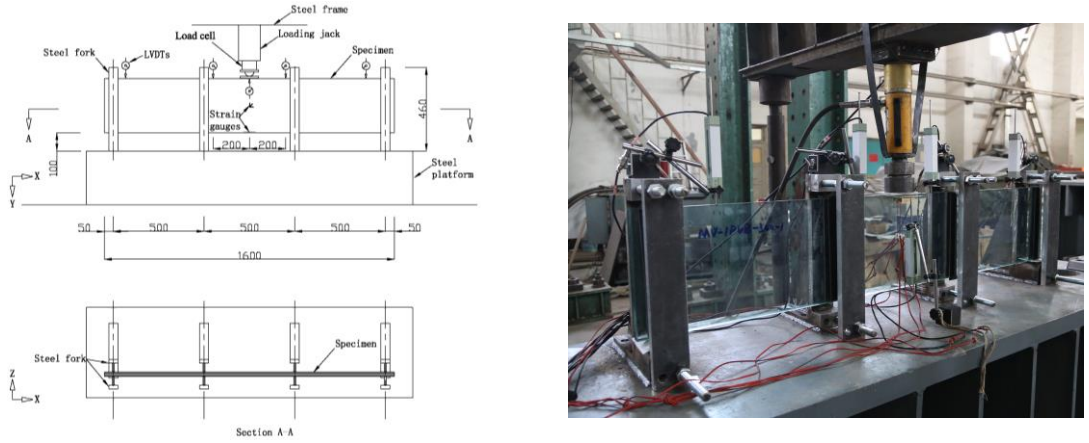

(a) Schematic diagram (b) Photo

Fig. 1 Test set-up

The LG specimens were tested in three-point bending. A schematic diagram of the test setup is shown in Fig. 1, in which the LG specimen is supported on two fork bearings specially designed to simulate a set of simple supports. Each fork bearing comprised of a steel half round and a pair of steel *T*-shaped sections. At both ends the specimen rested on the half rounds and was clamped in position by the webs of the *T* sections. The edges of the webs contacting the specimen were all rounded so as to enable the specimen to rotate freely about its weak axis. The specimen was therefore restrained from movement along the directions of *Y* and *Z* and rotation about the direction of *X*, but allowed to rotate about the directions of *Y* and *Z*. The coordinate system used is illustrated in Fig. 1, in which the axes of *X*, *Y* and *Z* correspond to the longitudinal direction of the specimen, the vertical direction, and the horizontal direction perpendicular to the specimen, respectively. The overall length of the specimen was 1600 mm. The distance from the center of one steel half round to the adjacent end of the specimen was 50 mm. The clear span of the specimen was therefore 1500 mm. To avoid buckling, the specimen was laterally supported by two additional steel forks at two intervals of 500 mm along the length. These two forks were made similar to the fork bearings but without half bearing rounds. The distance between the two T-sections within every fork was adjustable to accommodate varying thicknesses of the LG specimens. Loads were introduced by a 10 T hydraulic jack. At the loading point, a ball hinge was used between the loading jack and the specimen to ensure that the load was applied at the mid-span. Nylon strips with a thickness of 2 mm were used as cushions between the steel and the glass to prevent high stress concentration in the glass.

2.3 Test instrumentation and procedure

Data acquired from the tests consisted of applied loads, vertical displacements and elastic strains of the LG specimens near the mid-span. These data were measured respectively by a load cell, five LVDTs and a number of strain gauges. One LVDT was placed below the loading jack at the mid-span. The other four LVDTs were respectively placed on the top edge of the specimen at a distance of 200 mm from the mid-span and at a distance of 50 mm from the ends of the specimen. The accuracies of the load cell and the LVDTs were 0.1 kN and 0.01 mm, respectively. To

investigate the failure stresses of the LG specimens, a one-way strain gauge measuring bending tensile strain along the longitudinal direction of the specimen was attached at the mid-span of the bottom edge of each ply of glass with epoxy adhesive. The strain gauges were foil type, with a resistance of 120-ohm and a sensitivity of 2.18±1%. The testing data were obtained at a rate of one measurement per second. The tests were displacement controlled. Testing was continued beyond the peak load until the post failure strength of the specimens dropped to zero. Before glass breakage occurred, the loading jack moved approximately at a rate of 0.5 mm/min, while in the post-failure stage the loading jack moved approximately at a rate of 10 mm/min. This process was repeated for each test specimen.

Table 2 Test results

Specimens	t (mm)	h (mm)	F_{peak} (kN)	$\sigma_{g,\ failure}$ (N/mm^2)				M_e (kNm)	M_i (kNm)	$\frac{M_e}{M_i}$	$F_{post\ failure}$ (kN)	T (℃)
MV-1SG-150-1	23.77	149.8	6.3	26.0		26.8		2.36	2.35	1.00	1.9	18.2
MV-1SG-150-2	23.89	153.0	7.8	31.6		31.8		2.93	2.95	0.99	1.9	17.5
MV-2SG-150-1	23.31	151.4	12.6	50.5	52.3	53.1		4.73	4.63	1.02	3.5	18.3
MV-2SG-150-2	23.22	151.4	11.8	50.0	49.7	49.8		4.43	4.42	1.00	3.2	17.2
MV-3SG-150-1	23.65	150.8	11.0	48.0	36.9	47.2	47.0	4.13	4.01	1.03	5.2	18.2
MV-3SG-150-2	24.11	152.0	11.7	47.9	50.0	47.5	47.7	4.39	4.48	0.98	5.4	17.5
MV-1SG-200-1	23.82	203.0	15.8	38.6		34.8		5.93	6.00	0.99	2.8	19.0
MV-1SG-200-2	23.75	197.4	20.0	47.4		50.5		7.50	7.55	0.99	2.5	19.0
MV-2SG-200-1	23.61	200.4	18.2	48.4	46.6	37.9		6.83	7.00	0.98	5.3	18.7
MV-2SG-200-2	23.40	203.6	19.5	46.5	46.1	45.4		7.31	7.44	0.98	5.3	18.6
MV-3SG-200-1	24.14	201.2	18.5	40.0	41.9	44.8	46.2	6.94	7.04	0.99	6.8	19.8
*MV-3SG-200-2	23.96	200.8	-	-				-	-	-	-	-
MV-1SG-300-1	23.81	302.2	42.2	41.9		45.6		15.83	15.86	1.00	7.3	19.5
MV-1SG-300-2	23.95	301.2	45.4	45.3		49.6		17.03	17.18	0.99	7.0	19.6
MV-2SG-300-1	23.23	301.6	42.8	43.1	44.7	46.3		16.05	15.74	1.02	12.2	18.5
MV-2SG-300-2	23.57	301.8	53.0	55.2	56.4	56.4		19.88	20.04	0.99	12.9	19.5
MV-3SG-300-1	23.73	294.8	52.2	55.4	55.7	57.0	58.6	19.58	19.48	1.01	17.6	19.0
MV-3SG-300-2	23.58	294.4	39.2	41.2	41.7	43.3	44.6	14.70	14.54	1.01	19.8	19.6
MV-1PVB-150-1	23.54	151.2	9.9	44.1		40.5		3.71	3.79	0.98	0.1	18.2
MV-1PVB-150-2	23.75	149.6	7.0	25.9		34.5		2.63	2.68	0.98	0.3	17.4
MV-3PVB-150-1	23.41	152.6	7.5	29.7	34.8	31.8	23.9	2.81	2.73	1.03	0.9	17.5
MV-3PVB-150-2	23.56	148.2	13.1	49.1	55.5	62.2	54.4	4.91	4.77	1.03	0.5	17.4
MV-1PVB-300-1	23.78	302.8	45.7	49.7		46.4		17.14	17.46	0.98	0.4	19.5
MV-1PVB-300-2	23.69	301.0	40.9	45.3		40.3		15.34	15.31	1.00	0.6	20.0
MV-3PVB-300-1	23.58	296.8	34.8	38.6	41.0	38.5	32.8	13.05	13.06	1.00	1.9	20.2
MV-3PVB-300-2	23.66	303.4	42.6	43.0	42.8	44.7	44.1	15.98	15.84	1.01	2.6	19.7

*No results available due to technical problems

3. Test results

Table 2 presents the results in terms of load resistance (F_{peak}), failure stress ($\sigma_{g,failure}$), post failure load ($F_{post\ failure}$) and ambient temperature during testing for each specimen.

Since failures of the specimens were found to be all caused by vertical cracks initiated at the tensile edge near mid-span, the tensile stress generated by the F_{peak} was defined as the failure stress. By multiplying the measured tensile strain at failure with the Young's modulus (70000 N/mm^2) of the glass, the failure stress for each glass sheet was thus determined. It may be observed from Table 2 that the load resistance in some cases is somewhat different for the two nominally identical beams, such as MV-1SG-200 and MV-3PVB-150. This difference is mainly because of the relatively large variation in the failure stress of the glass samples, as can be shown by the measured failure stresses of the correlated glass samples. For example, the measured average failure stress of the MV-3PVB-150-1 is 30.1MPa, while that of the MV-3PVB-150-2 is 55.3MPa. As a result, the load resistance of the former is only 7.5kN, but that of the latter is 13.1kN. The scatter in the failure stress is mostly attributed to the random edge flaws in terms of sizes and distributions induced from manufacturing process.

The post-failure strength of the LG specimens was inferred by observation of load levels which, after dropping suddenly from a peak, started to increase again, as illustrated in Fig. 2 (e). The tests were carried out in an uncontrolled room with temperatures ranging from 17.2℃ to 20.2℃. Also given in Table 2 were the average measured glass thickness (t) and depth (d) of each

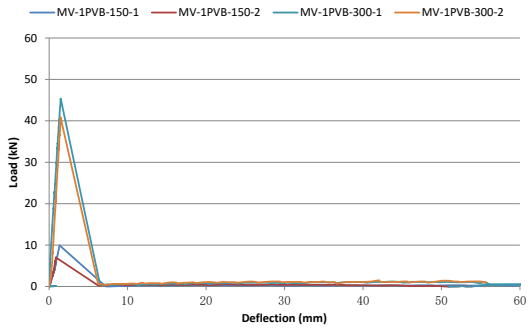

(a) PVB interlayer = 1

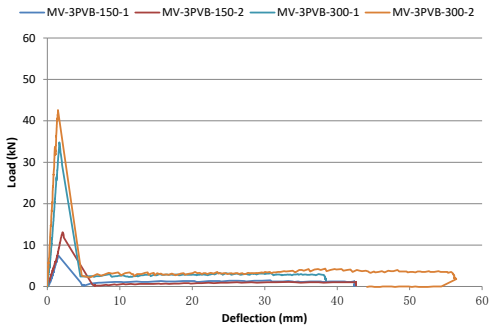

(b) PVB interlayer = 3

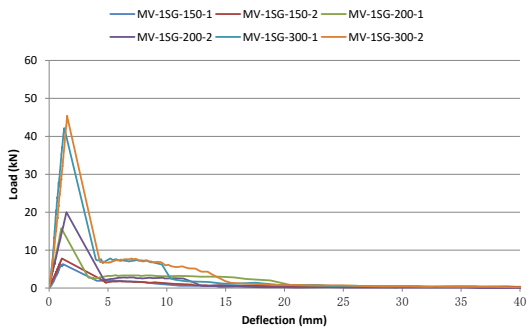

(c) SGP interlayer = 1

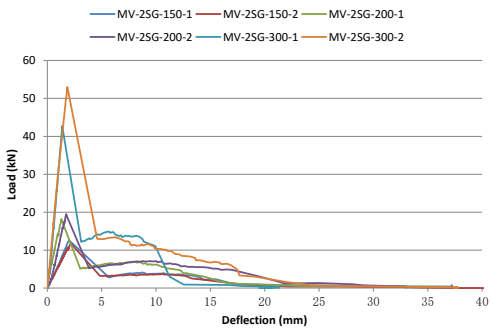

(d) SGP interlayer = 2

Fig. 2 Load-deflection curves of the LG specimens

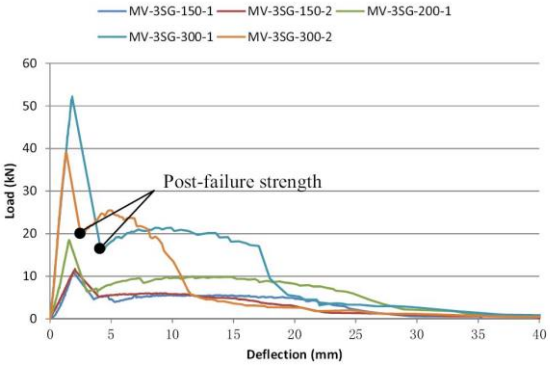

(e) SGP interlayer = 3

Fig. 2 Continued

specimen. The measurements were made respectively at the mid-span, quarter-span, and ends of each specimen. It should be noted that the individual glass thickness was not measured prior to lamination, thus the glass thickness (t) of each specimen was determined by deducting the nominal interlayer thickness from the measured overall thickness of the specimen.

The curves of applied loads against corresponding mid-span deflections of the LG specimens were plotted and are presented in Figs. 2(a)-(e). They were grouped into five graphs according to the type and number of interlayer used in the specimens. As can be seen from Figs. 2(a)-(e), the load-deflection curves of the LG specimens were all characterized by a linear elastic pre-failure stage, a sudden drop of load due to cracks which appear in the glass, and a nonlinear post-failure stage in which the cracks developed further until the interlayer ruptured.

4. Discussions

4.1 Influence of interlayers on the flexural stiffness

To examine whether interlayers have any significant influence on the flexural stiffness of LG, the load-deflection curves (in the linear stage) of the LG beam specimens with relatively high interlayer percentage, i.e. MV-3PVB and MV-3SG series, are respectively summarized in Figs. 3(a)-(d) to compare with the theoretical calculations that only consider the glass thickness but ignore the interlayer thickness. Since the structural behaviors of two nominally identical specimens were in good agreement in linear stage, only the curves of MV-3PVB-150-1, MV-3PVB-300-1, MV-3SG-150-1 and MV-3SG-300-1 were presented for ease of presenting the results. The theoretical load-deflection relationships of these specimens were calculated using the following equation based on the classic beam theory (Timoshenko 1956)

$$\delta = \frac{Fl^3}{48E_g I_g}\left(1+3.9\frac{h^2}{l^2}\right) \tag{1}$$

in which δ is the deflection at mid-span, F is the applied force, l is the effective span of the specimen, h is the cross-sectional depth of the specimen, E_g is the Young's modulus of the glass, I_g

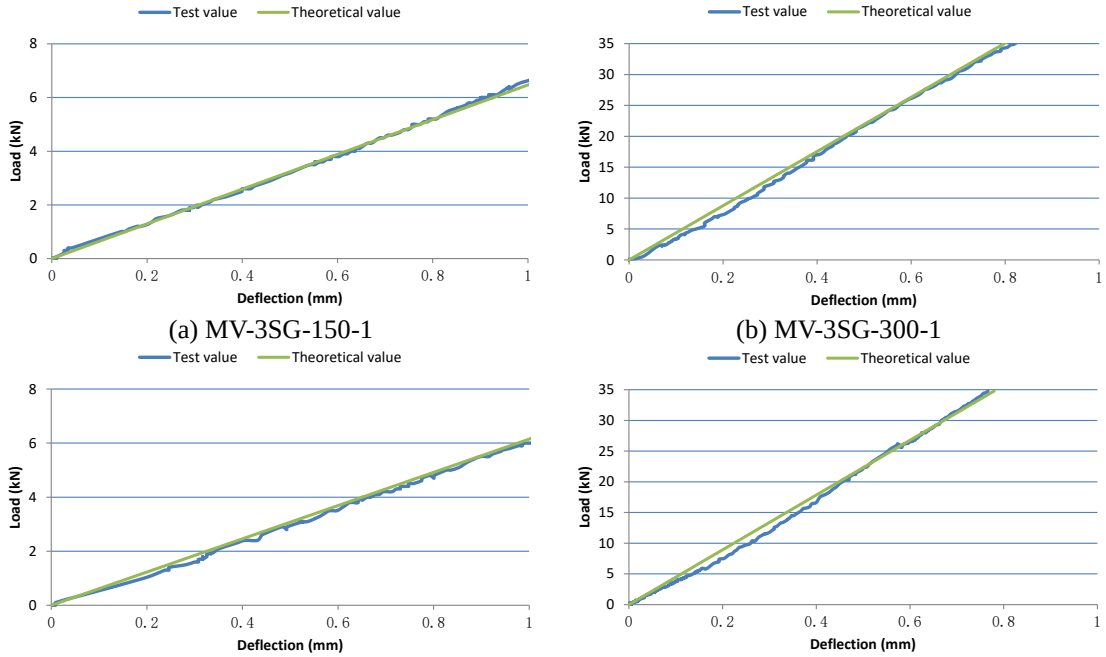

(a) MV-3SG-150-1 (b) MV-3SG-300-1

(c) MV-3PVB-150-1 (d) MV-3PVB-300-1

Fig. 3 Comparison of load-deflection curves in the linear stage between test results and theoretical calculations

is the moment of inertia of the cross section which is determined by the equation; $I_g = \frac{th^3}{12}$. The measured *t* and *h* were used in the calculation. Since the *h* to *l* ratios of the specimens can be up to 1/5, the effect of shear deformation was considered in the calculation. The comparison from Figs. 3(a)-(d) shows a good agreement between the theoretical predictions and the test results. Because the theoretical calculation only took into account the glass thickness and ignored the interlayer thickness, the close agreement indicates that neither the SGP nor the PVB interlayer had any significant effect on the flexural stiffness of the LG beam specimens. This observation results from the fact that the Young's modulus of the SGP or the PVB interlayer is a relatively small amount (only $1/10^3$~$1/10^5$) compared to that of the glass.

4.2 Influence of interlayers on the moment resistance

For a LG beam, its moment resistance provided by glass sheets and interlayer materials can be calculated as $\frac{2\sigma_{g,failure} I_g}{h} + \frac{2\sigma_{int} I_{int}}{h}$. Because no delamination was observed, according to the compatible condition it is rational to assume that at failure the maximum tensile stress in the interlayer (σ_{int}) can be calculated by $\frac{\sigma_{g,failure} E_{int}}{E_g}$. Since the Young's modulus of the interlayer (E_{int}) is only $1/10^3$~$1/10^5$ of the glass (E_g), it means that the σ_{int} is also $1/10^3$~$1/10^5$ of the $\sigma_{g,failure}$. Consequently the moment resistance provided by the interlayer can be rather insignificant

compared to that provided by the glass. In order to demonstrate this inference, the internal moment (denoted as M_i) provided solely by the glass sheets (ignoring the effect of interlayer materials) was compared with the external moment (denoted as M_e) generated by the applied load. The M_i was determined by $\frac{2I_g}{nh}\sum_{i=1}^{n}\sigma_{g,failure}^{i}$, where n is the number of the glass sheets. The M_e was determined by $\frac{F_{peak}l}{4}$. The values of $\sigma_{g,failure}^{i}$, F_{peak}, M_i, M_e, and the comparison between M_i and M_e for each specimen are provided in Table 2. As can be seen from the table, the values of M_i are very close to the corresponding values of M_e. The average difference was no more than 1% for either the SGP or the PVB LG beams. It was therefore confirmed that the SGP and PVB interlayer played a negligible role and their effects should be neglected in calculating the moment resistance of SGP and PVB LG beams.

4.3 Influence of shear force on the load resistance

In order to assess whether the presence of shear force has any significant influence on the load resistance of LG beams, the actual bending section capacity of the beams under combined bending and shear (denoted as M^*) was compared to the bending section capacity of the beams in pure bending (denoted as M_c). It is worth noting that the M^* actually is the same in value as the above mentioned M_e although different terms are used. In calculating the M_c, due to the bending tensile strength in the state of pure bending was unavailable, a design tensile strength ($\sigma_{g,design}$) of 25MPa was used instead with reference to the current codes of practice (JGJ113 2009; AS1288 2006; prEN16612 2013; ASTM E1300 2012). This value is applicable for annealed float glass subjected to short term loading. Consequently the M_c was determined by $\frac{2\sigma_{g,design}I_g}{h}$. The ratio of M^* to M_c against the shear span ratio was plotted for each LG specimen and presented in Fig. 4.

As is well known, shear forces can reduce the bending section capacity of a beam. Therefore, if the presence of shear force significantly affected the load resistance of the LG beams, the combined bending and shear section capacity M^* should be notably smaller in comparison with the pure bending section capacity M_c, especially for those LG beams with smaller shear span ratio. Seen from Fig. 4, however, it is found that no M^* is smaller than the corresponding M_c. The mean value of the M^* to M_c is approximately 1.75. One possible explanation for this observation is that like other brittle materials, such as concrete and ceramic, the shear strength of the glass can be relatively high compared to its tensile strength at failure. As a result, the level of the shear force in any of the LG beams was still low compared to the shear resistance of the beams, so that it had little effect on the load resistance of the LG beams. Fig. 4 also showed that in calculating the design bending section capacity, ignoring the effect of shear forces is rational and safe.

4.4 Failure patterns and post-breakage performance

Typical failure patterns of the PVB and SGP LG beams were identified from the tests and summarized in Figs. 5 (a)-(b). The characteristics of the two failure patterns were very different and thus resulted in very different post-breakage performances.

For the failure pattern of the PVB LG beams, the cracks initiated at the tensile edge and quickly propagated through the entire cross section of the LG beams. Due to this failure mechanism, the

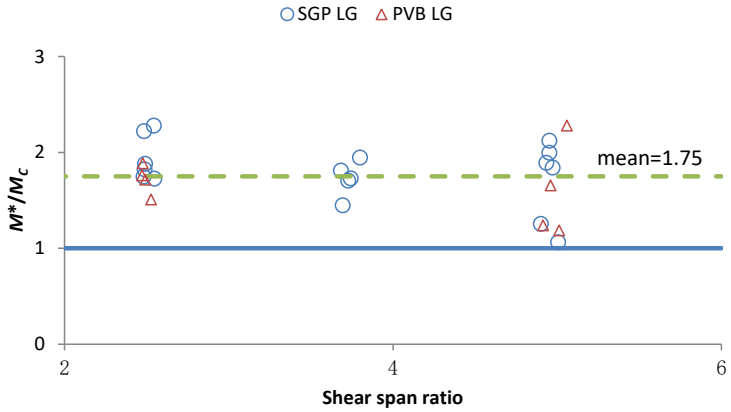

Fig. 4 Investigation of influence of shear force on the load resistance

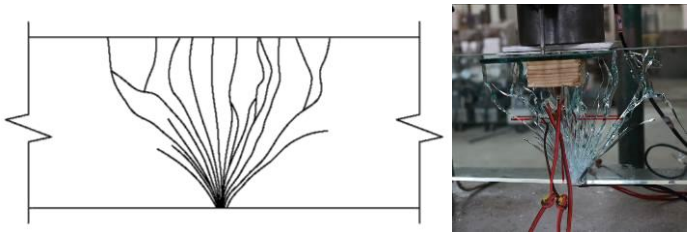

(a) PVB LG beams

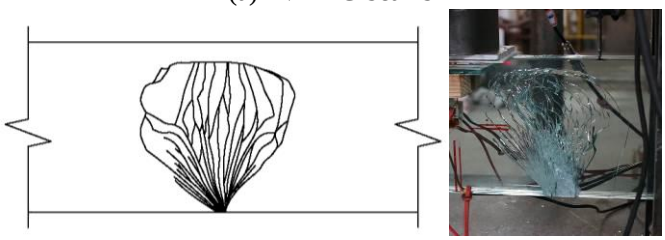

(b) SGP LG beams

Fig. 5 Typical failure patterns

PVB LG beams were found to have little post-breakage performance, as seen from Figs. 2 (a)-(b).

As for the failure pattern of the SGP LG beams, the cracks, whilst also initiating at the tensile edge, quickly formed into a diamond shape. Further growth of the cracks towards the compression zone was then effectively prevented by the interlayer, preventing the cracks from passing through the entire cross section of the LG beams. In this post-failure state a new load carrying mechanism in the beams was generated between the interlayer in the cracked tensile zone and the glass in the unbroken compressive zone to withstand the applied bending moment. As a result, the SGP LG beams were found to have notable post-breakage strength, as seen from Figs. 2 (c)-(e).

Based on this load carrying mechanism, a simplified analytical model was proposed to predict the post-breakage strength of the SGP LG beams. A schematic diagram of the analytical model is shown in Fig. 6.

It was assumed that after the glass broke, the SGP interlayer in the tensile zone carried the tensile forces in a fully plastic state. This assumption was made on the basis of two facts: firstly,

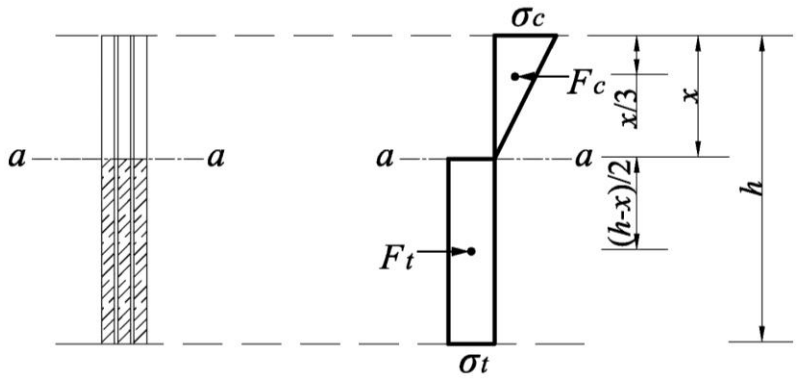

Fig. 6 Schematic diagram of stress distribution over the cross section of SGP LG beams in the post-failure stage

the SGP materials had an elastic-plastic behavior (with an initial yield strain of ≈8% and a failure strain of ≈350%) (DuPont 2008); secondly, the SGP materials overlapping the cracks very possibly underwent large stretch due to no local delamination being observed in the cracked zone. Consequently the following equations can be established based on the equilibrium condition

$$\frac{F_{post\ failure}l}{4} = F_t(\frac{h-x}{2} + \frac{2x}{3}) \tag{2}$$

$$F_t = \sigma t(h-x) \tag{3}$$

in which F_t is the resultant tensile force provided by the SGP interlayer, x is the height of the compression zone, t is the overall thickness and σ is the yield tensile stress of the SGP interlayer.

By substituting Eq. (3) into Eq. (2), the post-failure strength of a SGP LG beam can then be expressed as a function with respect to the value of x

$$F_{post\ failure} = \sigma t \frac{(2h^2 - \frac{4}{3}hx - \frac{2}{3}x^2)}{l} \tag{4}$$

It should be noted that the value of x is correlated to the ambient temperature and loading duration due to the visco-elastic properties of the SGP interlayer. Through examining the un-cracked compression zone of each SGP LG beam, it was suggested that the value of x may be taken as $0.1h$, for the SGP LG beams carrying short term loads at room temperature. Eq. (4) can thus be reduced to

$$F_{post\ failure} = \frac{281\sigma th}{150} \times \frac{h}{l} \tag{5}$$

Eq. (5) revealed that increasing the thickness of the SGP interlayer or the depth of the cross section can increase the post-failure strength of a SGP LG beam, whereas increasing the shear span ratio can reduce the post-failure strength of the SGP LG beam. These analytical predictions can be verified by the test results, as illustrated in Figs. 7 (a)-(c).

For the SGP interlayer subjected to short term loading at room temperature, its engineering

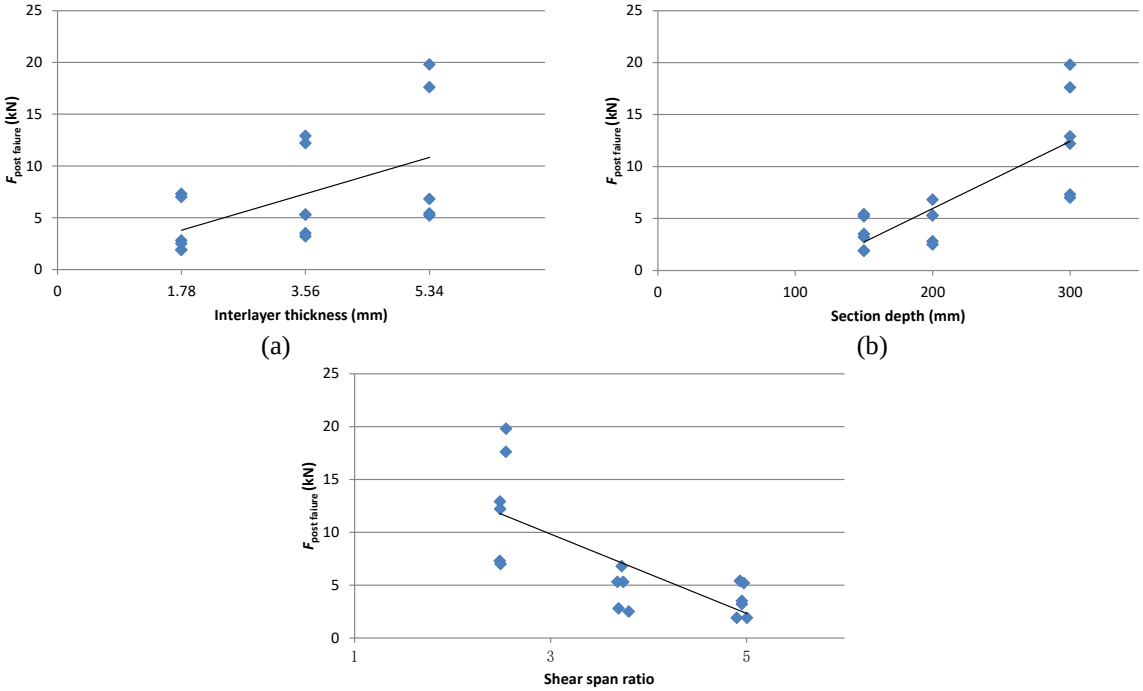

Fig. 7 Varying of the post-failure strength with respect to (a) the interlayer thickness, (b) section depth, and (c) shear span ratio of the SGP LG beams

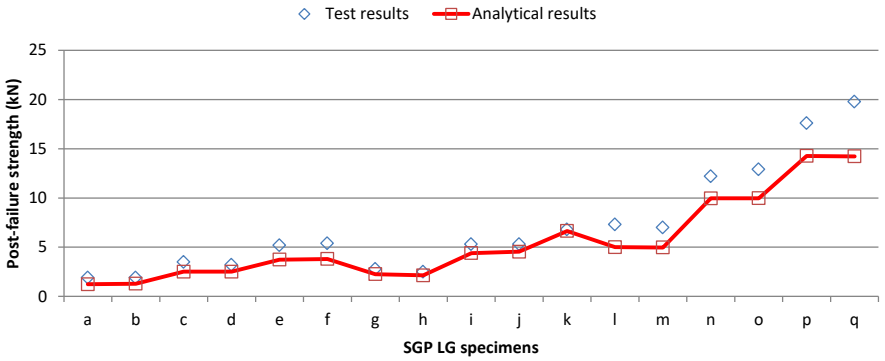

Fig. 8 Comparison of post-breakage strengths obtained from tests and analytical prediction

yield stress (σ_{eng}) and engineering initial yield strain (ε_{eng}) were approximately 23 N/mm^2 and 8%, respectively (DuPont 2008). As large strain behavior was involved, the σ_{eng} and ε_{eng} were converted into true yield stress, which was $\sigma=\sigma_{eng}(1+\varepsilon_{eng})$=24.8 N/mm^2. Substituting this value into Eq. (5), the post-breakage strength can thus be determined.

Using this method, the post-breakage strength of each SGP LG beam was calculated and presented in Fig. 8 to compare with the post-breakage strength obtained by the tests. The seventeen SGP LG beams listed in Table 2 were labeled a-q from the top down. The ratios of the test results to the predicted results were found in a range from 1.0 to 1.5, with a mean value of 1.2 and

standard deviation of 0.1. The predicted results can therefore be deemed as a reasonable lower bound of the test results, as shown in Fig. 8.

5. Conclusions

This paper presents an experimental study into the in-plane structural behavior of LG beams made up of multi-layered glass sheets. A range of 26 LG specimens were subject to short term three-point bending at room temperature. The investigated parameters included interlayer type, interlayer number, cross-sectional interlayer percentage, and shear span ratio of the LG beam specimens. The study was focused on the flexural stiffness, load resistance of the LG beams prior to failure, as well as on their post-failure behaviors in terms of failure pattern and post-failure strength. To this end the load-deflection response, failure tensile stress, and typical failure mode were recorded and examined for each LG beam specimen. The load-deflection curves of the LG beam specimens were found to all be characterized by a linear elastic pre-failure stage, a sudden drop of load due to glass cracking, and a nonlinear post-failure stage allowing for crack propagation until the interlayer ruptured. Furthermore, the following conclusions can be drawn from the study:

- Neither SGP nor PVB interlayer had any appreciable influence on the flexural stiffness and load resistance of the LG beams, even for those LG beams having a cross-sectional interlayer percentage as high as 18%.
- The failures of the LG beam specimens were all induced by excessive bending tensile stress at the tension edge of the beams. As long as the shear span ratio of the LG beams was not less than 2.5, the presence of shear force appeared to have little effect on the load carrying capacity of the LG beams.
- The typical failure patterns for the PVB and SGP LG beams were respectively identified.
- The PVB LG beams were found to have poor post-failure performance whereas the SGP LG beams had notable post-failure performance due to different failure mechanisms.
- The post-failure strength of the SGP LG beams can be effectively enhanced by increasing the interlayer thickness or the depth of the cross section, but is reduced by increasing the shear span ratio.
- A simple engineering model was developed to predict the post-failure strength of the SGP LG beams. After comparison with the test results, the simple model was deemed to be reasonable in predicting the post-failure strength.

Acknowledgments

Kuraray (Shanghai) Co. Inc. and Fuxin Special Glass (China) Co. Inc. are gratefully acknowledged for providing the LG testing specimens.

References

Amadio, C. and Bedon, C. (2010), "Buckling of laminated glass elements in out-of-plane bending", *Eng. Struct.*, **32**, 3780-3788.

AS 1288 (2006), Glass in buildings - selection and installation, Sydney.
Aşik, M.Z. and Tezcan, S. (2005), "A mathematical model for the behavior of laminated glass beams", *Comput. Struct.*, **83**, 1742-1753.
ASTM E1300 (2012), Standard practice for determining load resistance of glass in buildings, New York.
Behr, R., Minor, J. and Norville, H. (1993), "Structural behavior of architectural laminated glass", *J. Struct. Eng.*, **119**, 202-220.
Belis, J., Bedon, C., Louter, C., Amadio, C. and Van Impe, R. (2013), "Experimental and analytical assessment of lateral torsional buckling of laminated glass beams", *Eng. Struct.*, **51**, 295-305.
Belis, J., Depauw, J., Callewaert, D., Delincé, D. and Van Impe, R. (2009), "Failure mechanisms and residual capacity of annealed glass/SGP laminated beams at room temperature", *Eng. Fail. Anal.*, **16**(6), 1866-1875.
Biolzi, L., Cattaneo, S. and Rosati, G. (2010), "Progressive damage and fracture of laminated glass beams", *Constr. Build. Mater.*, **24**, 577-584.
Bos, F. and Veer, F. (2007), "Consequence-based safety requirements for structural glass members", *Proceedings of Glass Processing Days*, Tampere, Finland.
Callewaert, D., Belis, J., Delincé, D. and Van Impe, R. (2012), "Experimental stiffness characterisation of glass/Ionomer laminates for structural applications", *Constr. Build. Mater.*, **37**, 685-692.
DuPont de Nemours (2008), SentryGlas Plus elastic properties (SGP5000), DuPont.
Duser, A.V., Jagota, A. and Bennison, S.J. (1999), "Analysis of glass/polyvinyl butyral laminates subjected to uniform pressure", *J. Eng. Mech.*, **125**(4), 435-442.
Foraboschi, P. (2007), "Behavior and failure strength of laminated glass beams", *J. Eng. Mech.*, **133**(12), 1290-1301.
Huang, X.K., Liu, G., Liu, Q. and Bennison, S.J. (2014), "An experimental study on the flexural performance of laminated glass", *Struct. Eng. Mech.*, **49**(2), 261-271.
Huang, X.K., Liu, G., Liu, Q. and Bennison, S.J. (2014), "The flexural performance of laminated glass beams under elevated temperature", *Struct. Eng. Mech.*, **52**(3), 603-612.
Huang, X.K., Liu, G., Liu, Q. and Bennison, S.J. (2015), "Influence of interlayers on the flexural performance of four-side supported laminated glass at room temperature", *Adv. Struct. Eng.*, **18**(1), 33-43.
JGJ 113. (2009), Technical specification for application of architectural glass, Beijing.
Kott, A. and Vogel, T. (2003), "Remaining structural capacity of broken laminated safety glass", *Proceedings of Glass Processing Days*, Tampere, Finland.
Ledbetter, S., Walker, A. and Keiller, A. (2006), "Structural use of glass", *J. Arch. Eng.*, **12**(3), 137-149.
Luible, A. and Crisinel, M. (2006), "Design of glass beams subjected to lateral torsional buckling", *Proceedings of the IABSE Symposium "responding to tomorrow's challenges in structural engineering"*, Budapest, Hungary.
prEN 16612 (2013). Glass in building - determination of the load resistance of glass panes by calculation and testing, London.
Seshadri, M., Bennison, S., Jagota, A and Saigal, S. (2002), "Mechanical response of cracked laminated plates", *Acta Materialia*, **50**(18), 4477-4490.
Timoshenko, S. (1956), *Strength of Materials, Part I*, 3rd Edition, Van Nostrand Reinhold Company, New York, USA.
Wurm, J. (2007), *Glass Structures: Design and Construction of Self-supporting Skins*, Birkhäuser Verlag AG, Basel, Boston, Berlin.

CC